Gems of the Galaxy Zoos - a Wide-Ranging *Hubble Space Telescope* Gap-Filler Program[*]

William C. Keel,[1] Jean Tate,[2] O. Ivy Wong,[3,4] Julie K. Banfield,[5] Chris J. Lintott,[6] Karen L. Masters,[7] Brooke D. Simmons,[8] Claudia Scarlata,[9] Carolin Cardamone,[10] Rebecca Smethurst,[6] Lucy Fortson,[9] Jesse Shanahan,[11] Sandor Kruk,[12,13] Izzy L. Garland,[8] Colin Hancock,[1] and David O'Ryan[8]

[1]*Department of Physics and Astronomy, University of Alabama, Box 870324, Tuscaloosa, AL 35487*
[2]*Private address[b]*
[3]*CSIRO Space & Astronomy, PO Box 1130, Bentley, WA 6102, Australia*
[4]*ICRAR-M468, University of Western Australia, Crawley, WA 6009, Australia*
[5]*Research School of Astronomy and Astrophysics, Australian National University, Canberra, ACT 2611, Australia*
[6]*Department of Physics, University of Oxford, Denys Wilkinson Building, Keble Road, Oxford OX1 3RH, UK*
[7]*Departments of Physics and Astronomy, Haverford College, 370 Lancaster Ave, Haverford, PA 19041*
[8]*Physics, Lancaster University, Lancaster LA1 4YB, UK*
[9]*School of Physics & Astronomy, University of Minnesota, 116 Church Street S.E., Minneapolis, MN 55455*
[10]*Center for the Enhancement of Learning and Teaching, Tufts University, 108 Bromfield Road, Somerville, MA 02144*
[11]*Center for Astrophysics and Space Sciences (CASS), Department of Physics, University of California, San Diego, CA 92093, USA*
[12]*European Space Agency, ESTEC, Keplerlaan 1, NL-2201 AZ Noordwijk, the Netherlands*
[13]*Max-Planck-Institut für extraterrestrische Physik (MPE), Giessenbachstraße 1, D-85748 Garching bei München, Germany"*

ABSTRACT

We describe the Gems of the Galaxy Zoos (Zoo Gems) project, a gap-filler project using short windows in the *Hubble Space Telescope*'s schedule. As with previous snapshot programs, targets are taken from a pool based on position; we combine objects selected by volunteers in both the Galaxy Zoo and Radio Galaxy Zoo citizen-science projects. Zoo Gems uses exposures with the Advanced Camera for Surveys (ACS) to address a broad range of topics in galaxy morphology, interstellar-medium content, host galaxies of active galactic nuclei, and galaxy evolution. Science cases include studying galaxy interactions, backlit dust in galaxies, post-starburst systems, rings and peculiar spiral patterns, outliers from the usual color-morphology relation, Green Pea compact starburst systems, double radio sources with spiral host galaxies, and extended emission-line regions around active galactic nuclei. For many of these science categories, final selection of targets from a larger list used public input via a voting process. Highlights to date include the prevalence of tightly-wound spiral structure in blue, apparently early-type galaxies, a nearly complete Einstein ring from a group lens, redder components at lower surface brightness surrounding compact Green Pea starbursts, and high-probability examples of spiral galaxies hosting large double radio sources.

1. INTRODUCTION

Corresponding author: William C. Keel
wkeel@ua.edu

Astronomy enjoys a rich history of knowledge gained from objects at the extremes of sample properties, and outliers to common correlations. Our experience with spinoff studies from the Galaxy Zoo projects has certainly borne this out, leading to further observation of rare and unusual galaxies which in turn yielded insight in a range of questions in galaxy evolution. This paper describes one such project, delivering *Hubble Space Telescope* (HST) images of galaxies randomly selected from a list chosen for science value in a number of contexts.

Galaxy Zoo has encompassed several iterations of classification based on volunteer examination of galaxies in digital sky surveys. Initially, "classic" Galaxy Zoo (Lintott et al. 2008) provided broad morphological information (spiral/elliptical/merging, and direction of spiral arms) for over 900,000 galaxies from data release 7 (DR7, Abazajian et al. 2009) of the Sloan Digital Sky Survey (SDSS; York et al. 2000). Galaxy Zoo 2 (Willett et al. 2013) built on the demonstrated ability of volunteers to consistently provide finer-grained morphological information, now working with about 250,000 of the brightest SDSS galaxies. The approach was extended, broadening the decision tree to encompass clumpy galaxies, to deep optical HST fields in Galaxy Zoo Hubble (Willett et al. 2017) and the near-IR CANDELS data (Simmons et al. 2017), and most recently images from the Legacy Survey (Dey et al. 2019). The results of these studies led to recognition of the importance of blue early-type galaxies (blue ellipticals for short; Schawinski et al. 2009a) and red spiral galaxies (Masters et al. 2010, Bamford et al. 2009); Masters et al. (2020) summarizes the first twelve years of Galaxy Zoo results. It quickly became clear that the project discussion forum[1], where volunteers could ask questions and exchange comments about galaxy images, was drawing attention to very rare phenomena, leading to the identification of Green Pea compact starburst systems (Cardamone et al. 2009), nearly 2000 pairs of galaxies with overlapping images for dust analysis (Keel et al. 2013), and giant extended emission-line regions (EELRs) around active galactic nuclei (AGN), many of which are so luminous as to suggest that the central AGN must have faded within the relevant light-travel time (Lintott et al. 2009, Keel et al. 2012a). Beyond these, numerous other galaxy images of special interest have been brought up for discussion on the Forum and its successor in the project's Talk interface[2], providing ready sets of objects for followup observation. As this became clear, team members could call for specific kinds of objects, and were often answered with great energy by volunteers. Beyond the primary statistical goals of the various iterations of the Galaxy Zoo public-participation project, some of its hundreds of thousands of volunteer participants have identified rare and unusual galaxies for which further data would be particularly interesting.

The more recent launch of Radio Galaxy Zoo (Banfield et al. 2015), in which participants examine optical and near-infrared images in concert with radio data, likewise makes use of the Talk interface for exchange of more detailed information, particularly on the rare radio galaxies with possibly spiral host morphology and on active galactic nuclei (AGN) with extensive emission-line clouds. For many of the objects, their nature would become much clearer with higher-resolution optical images than the SDSS data used for the initial rounds of Galaxy Zoo classifications, and numerous specific science goals could be addressed with even a modest set of such followup images.

Galaxy Zoo team members had long joked about the appropriate followup observing proposal being "We have a bunch of weird galaxies, and need a closer look to understand them better". This was essentially what the 2017 STScI gap-filler opportunity offered. We describe in this paper the resulting program, "Gems of the Galaxy Zoos" (Zoo Gems for short, program 15445), which has provided HST images relevant to a wide range of science cases drawn from Galaxy Zoo and Radio Galaxy Zoo. In this paper, we describe these aims, detail how we incorporated public input in selecting the target lists for many of the science cases we could address, document the setup of the observations, and present some initial results. While many of the results of Zoo Gems will appear in further papers, we think it useful to provide here the common background and rationale of the observations.

2. SCIENCE CASES

This section sets out the science rationales for various object categories, organized into broad morphological themes. Some categories have had only a single example observed at this point.

2.1. *Galaxy disks*

2.1.1. *Galaxy Zoo: unusual spirals*

This category furnishes a catchall for spiral galaxies - 3-armed grand-design systems, galaxies with very asymmetric patterns but no obvious interacting companion, or dominant resonance ring structures. The 3-armed spirals took on

---

[1] https://www.galaxyzooforum.org/, with content frozen 9 July 2014

[2] https://talk.galaxyzoo.org/ until April 2019, discussion moved to https://www.zooniverse.org/projects/zookeeper/galaxy-zoo/talk thereafter.

particular interest with the finding from Galaxy Zoo 2 classifications that they are not more common in low-density environments, as had been expected from relative growth properties of various Fourier modes (Elmegreen et al. 1992, Durbala et al. 2009), and that bars are just as common in these as in the 2-armed examples where the 180° symmetry of bar and arms matches (Hancock 2019).

2.1.2. *Galaxy Zoo: nuclear disks and bars in spirals*

High-resolution images have shown some spiral galaxies, especially those with bars and outer rings, to have analogous circumnuclear structures - known as nuclear disks. We included galaxies seen (or very likely) to have unusually large central disks within bars, or central bars misaligned with the outer structures.

2.1.3. *Galaxy Zoo: backlit galaxies*

Noninteracting galaxy pairs whose images overlap in projection offer a way to study dust attenuation independent of dust temperature or structure of the galaxy, and subject to completely different systematics than methods relying on IR emission or modeling of the galaxy's spectral-energy distribution (SED). This approach has been applied to very limited sets of galaxies, using ground-based data by White & Keel (1992), Berlind et al. (1997), and White et al. (2000), and with the improved angular resolution of HST imaging by Elmegreen et al. (2000) Keel & White (2001), Keel & White (2001) and Holwerda et al. (2009). Applicability of this technique remained limited by the very modest number of suitable backlit galaxies then known, a situation which was dramatically improved by the sensitivity and (especially) dynamic range of SDSS data. Galaxy Zoo participants provided an extensive finding list of candidate pairs, for a catalog of nearly 2000 such pairs after validation from their initial examination of DSSS DR7 images alone (Keel et al. 2013). This list has been supplemented by the second pass through DR7 images during Galaxy Zoo 2. Similar pairs were also noted during Hubble Zoo, but not considered here since Zoo Gems images would not improve their data quality. The ideal pair would have galaxies with redshifts so different as to rule out physical association, containing a smooth early-type galaxy behind a relatively symmetric spiral. In practice these criteria can be relaxed, for example to include pairs with particular geometries or evidence for very distant attenuation regions, as long as the image information is properly used to estimate uncertainties due to departures from symmetry.

2.2. *Starbursts and star-forming regions*
2.2.1. *Galaxy Zoo: Green Peas*

Green Pea systems, as described by Cardamone et al. (2009), were initially identified as a class by Galaxy Zoo volunteers. The name arises from their combination of small size (SDSS Petrosian radius $petrorad\_r < 2.0''$) and green appearance in SDSS gri composite images, arising from a strong emission line in the r band (refined to $ugriz$ color criteria by Cardamone et al. 2009). The dominant emission line for these "green" objects is redshifted [O III] $\lambda5007$. Inspection of the SDSS spectra showed most of these to be star-forming systems; their small angular sizes and redshifts meant these are therefore among the most compact star-forming galaxies, and the large emission-line equivalent widths responsible for their color selection mark them firmly as starburst systems. Only a handful of Green Peas appeared serendipitously in previous HST imagery, so we incorporated Peas into the Zoo Gems list to enable a more systematic study of their structures. In particular, we selected filters that emphasized the stellar continuum, for a better view of the structure of the galaxies themselves, and included systems in three redshift slices. Improved measurements or limits on the sizes of the stellar structures would lead to better understanding of how intense the starbursts are, and to what extent these extreme star-forming regions reside in systems with previous histories of star formation, or show evidence of tidal disturbance which could trigger these extreme starbursts. These red ACS WFC passbands also provide a contrast with the UV bands previously observed for some Green Pea samples using HST, which represent the young starburst populations well but not any older stellar components.

The Galaxy Zoo sample of Green Peas has generated extensive followup work as sources of Lyman-continuum leakage (Yang et al. 2017, Malkan & Malkan 2021), Lyman α emission sources (Orlitová et al. 2018), extreme starbursts driving global winds (Jaskot et al. 2017, Bosch et al. 2019, Hogarth et al. 2020), and testbeds for chemical evolution scenarios at high star-formation rates (Hawley 2012, Amorín et al. 2012). These compact, intense starbursts are likely related to the less massive "Little Blue Spheroids" (Moffett et al. 2019).

2.2.2. *Galaxy Zoo: Poststarbursts*

Spectroscopically-selected post-starburst galaxies[3] (using the combination of Hδ in absorption with equivalent width > 3 Å and Hα emission undetected at the 4σ level) show central concentrations (SDSS *fracdev* parameter) intermediate between disk and early-type galaxies (Wong et al. 2012). This could reflect genuine morphological transformation or preferential scales for the starburst, both issues which higher-resolution images could shed light on. This selection on specific absorption line properties is distinct from the color/luminosity selection often defining the "Green Valley", being influenced by star-formation events which are more localized or involve smaller gas masses, but the possibility of post-starburst systems being seen during morphological transformation does parallel the inferences about galaxies in the Green Valley largely undergoing a one-time morphological change (Mendez et al. 2011, Schawinski et al. 2014, Smethurst et al. 2015, Kelvin et al. 2018). In addition, the fading starbursts are often concentrated in knots, which are often well-detected in snapshot observations, allowing broad comparison of the starburst properties. These properties in combination could suggest to what extent processes in local post-starburst galaxies are, or are not, useful analogs for the quenching of star formation in the galaxy population more generally.

2.2.3. *Galaxy Zoo: blue ellipticals*

One of the earliest Galaxy Zoo science results was the existence of galaxies robustly classified as early-type, with colors much bluer than the usual red sequence (Schawinski et al. 2009a), indicating an unusual level of recent star formation or contamination by the light of an AGN. High-resolution images can trace the distribution of star-forming regions, indicating whether they form disks, rings, or the kinds of asymmetric patches that could be infalling star-forming regions. We tracked three separate subcategories among blue ellipticals (selected using a color cut based on the red sequence track, as in Schawinski et al. 2009a), so the final list included the highest-ranked examples of blue early-type galaxies with emission-line ratios from SDSS spectra indicating that AGN or star formation is dominant (5 and 4 targets, respectively), and star-forming examples with detected CO or H I emission (3 targets; Schawinski et al. 2009b, Wong et al. 2015).

2.2.4. *Galaxy Zoo: Red spirals*

Analogous to blue ellipticals, Galaxy Zoo classifications led to identification of a population of red spiral galaxies (Masters et al. 2010), defined by color offset from typical spirals at a given luminosity. While present in all environments, they are most abundant in the high-density regions just outside cluster cores (Bamford et al. 2009). Galaxies for voting were selected to be nearly face-on, so the red color is not due solely to attenuation in the disk. The HST images could show whether the star-forming regions in these systems are of unusually low luminosity or unusually sparse compared to spirals of typical colors, and address the incidence of bars at small scales for comparison with the global bars which are common in these systems (Masters et al. 2011, Kruk et al. 2018). The properties of red spirals may give clues to the processes quenching star formation when seen independently of morphological transformations.

2.2.5. *Galaxy Zoo: luminous star-forming clumps in galaxies*

While rare in the local Universe, these may be helpful analogs to the luminous star-forming clumps which are ubiquitous in the high-redshift galaxy population (Cowie, Hu, & Songaila 1995, Elmegreen, Elmegreen, & Sheets 2004). The relative handful of nearby analogous objects will be much better resolved, providing information on scales of star formation (and sometimes the properties of the most luminous clusters in these regions).

2.3. *Interacting and merging galaxies*

2.3.1. *Galaxy Zoo: mergers which are very distorted or have very long/luminous tails*

Among the many interacting and merging systems flagged by Galaxy Zoo (Darg et al. 2010), some stand out even in such exceptional company as having tidal tails of unusual length or brightness, or main galaxy bodies which are unusually distorted. We include some of these in the target list, to sample the properties of galaxy interactions which produce such extreme stages. Outcomes might include populations of luminous star clusters, morphological information on scales beyond the SDSS resolution limit, and the role of dust attenuation (which can change our interpretation of a system's components and their spatial relationships).

---

[3] As it happened, all of the galaxies in this input list were affected by an initial bug in SDSS DR7 redshifts, which applied to galaxies having strong Balmer absorption lines and gave erroneously high redshifts when the gaps between Balmer absorption lines were matched to broad emission features. This was quickly corrected in the SDSS pipeline, before the release of DR8, and did not affect our sample construction.

2.3.2. *Galaxy Zoo: collisional and polar rings (including possible lenses)*

Numerous candidates for these rare interaction signatures were noted by Galaxy Zoo participants. They offer particular insight into not only the prevalence of these kinds of galaxy encounters, but such disparate issues as the shapes of dark-matter halos, properties of star formation with time mapped to location, and the degree of self-gravitation in polar rings (Reshetnikov & Combes 1994, Bizyaev et al. 2007, Egorov & Moiseev 2019). The top-voted polar-ring candidate was earlier catalogued as PRC A-1 in the catalog by Whitmore et al. (1990), supporting the identification of this system as hosting a classic polar-ring structure. This category also includes objects which may turn out to be gravitationally lensed arcs when examined at high angular resolution, as indeed happened in one spectacular and near-complete Einstein ring (section 5.5).

2.3.3. *Galaxy Zoo: Red/blue pairs*

Particularly in the earliest examination of Legacy Survey images (Dey et al. 2019), participants have found a small category of close pairs of marginally resolved images with very different colors. At first we suspected these might be star/galaxy superpositions, but one Zoo Gems image shows at least some to be interesting galaxy interactions, of the general kind long discussed as mixed-morphology pairs (Rampazzo & Sulentic 1992, Hernández Toledo et al. 1999) with contrasting morphologies, colors, and star-forming properties.

2.3.4. *Galaxy Zoo: regrowing disks*

The "merger hypothesis" for making elliptical galaxies by merging disk systems (Toomre 1977) was largely suggested by the tendency for disk mergers in simulations to yield elliptical-like, diskless remnants for mass ratios near unity (in practice, a cutoff near 3:1 has often been taken to give the right fraction of mergers, if not always the right outcomes in individual cases when such parameters as approach geometry and gas fraction are added to the mass ratio). However, as merger simulations achieve higher fidelity and are run for more combinations of the numerous initial conditions, some mergers of near-equal mass galaxies are shown to retain disks afterward (Barnes & Hernquist 1996, Governato et al. 2009, Hopkins et al. 2009). In parallel, we have noticed a category of interacting-galaxy pairs which show single disks and spiral patterns surrounding two distinct bulges, which could represent this process in action (and existence of a remnant disk before the nuclei merge). We included all these systems in the Zoo Gems object list, to give the possibility of empirical information on the survival or re-formation of disks in major mergers. Such events may be important in producing the population of high-luminosity "super spiral galaxies" identified by Ogle et al. (2016) and Ogle et al. (2019). They note that a significant fraction of these gigantic disk systems show signs of at least minor meters; retaining or regrowing disks after some major mergers would make it easier to understand the existence of disk-dominated systems at the highest galaxy luminosities.

2.4. *Active galactic nuclei and their host galaxies*
2.4.1. *Galaxy Zoo: EELRs*

Galaxy Zoo participants have proven to be adept at identifying candidates for extended emission-line regions (EELRs) associated with AGN, based on the distinctive colors in the SDSS *gri* composite images produced by strong [O III] emission appearing in g or r at different redshifts (Lintott et al. 2009, Keel et al. 2012a). The distance of these clouds from the AGN, and their luminosity compared to what we see from the AGN directly, constrain both the duty cycle of rapid accretion and characteristic duration of accretion episodes. Fine structure in these clouds strengthens constraints on the required ionizing luminosity of the associated AGN (Keel et al. 2012b, Keel et al. 2017), motivating us to include the strongest EELR candidates in filters matching the SDSS detection bands, even in the absence of separate HST continuum data.

2.4.2. *Radio Galaxy Zoo: EELRs*

As in Galaxy Zoo, Radio Galaxy Zoo participants identified many galaxies, or galaxy components, with such extreme colors that there are almost certainly strong, resolved emission-line clouds (some tagged as "RGZ Green" objects, since many are at redshifts $z \approx 0.25$ where [O III] emission appears in the r band, mapped to green in the SDSS and analogous color-composite displays). For radio-loud AGN, in addition to photoionization, emerging jets add the possibility of shock ionization on large scales. Here again, we specified filters closely matching the detection band from Radio Galaxy Zoo. The input list for voting incorporated both SDSS colors of the host and spatially resolved structure in the r filter.

2.4.3. *Radio Galaxy Zoo: SDRAGNs*

For convenience, we follow Leahy (1993) in using DRAGNS (Double-lobed Radio sources Associated with Galactic Nuclei) to describe typical double-lobed radio galaxies. A long-known property of the population of galaxies hosting DRAGNs is that they are overwhelmingly elliptical galaxies or merger remnants. However, detailed study has revealed a handful of galaxies, associated at high probability with DRAGNs, with clear spiral structure (Ledlow et al. 2001, Keel et al. 2006, Hota et al. 2011, Mao et al. 2015, Mulcahy et al. 2016) We will call these rare DRAGNs with spiral host galaxies SDRAGNs. We concentrate on these because they go against the dominant correlation of luminous double sources with elliptical or post-merger host galaxies, offering the possibility of a way to understand which host-galaxy properties drive (or allow) production of large-scale double sources. The initial list was selected based on location of the putative host galaxy with respect to the radio lobes, and evidence of a disk (a large exponential-disk fraction in the SDSS image analysis or from a full 2-dimensional fit to the SDSS images using GALFIT (Peng et al. 2002)).

The angular resolution of HST imaging can make the morphology of these galaxies, many as distant as $z \approx 0.2$, much clearer, resolving spiral arms, dust lanes, and star-forming regions, allowing a much more confident morphological assessment than the photometric bulge-disk decompositions that were our starting points. By the same token, the bulge properties will also be much better determined, giving an improved understanding of likely black-hole masses and evolutionary paths of these galaxies. For those radio sources which actually arise in a more distant galaxy than the spiral observed, improved astrometry with the HST data can identify such false associations.

2.5. *Galaxy Zoo: unusual bulges*

This category includes bulges which are unusually shaped, unusually prominent for the galaxy's morphological type, or appear prolate with respect to the disk orientation. The latter may indicate that the disk is more like a polar ring, resulting from material starting in a second galaxy. An important subtype is formed by so-called X-bulges (extreme versions of "peanut bulges") which have attracted attention as being edge-on views of bars, allowing us to visualize the distribution of stars along a direction which remains unseen in images of more face-on systems (Bureau & Freeman 1999, Kruk et al. 2019).

3. FINAL TARGET LIST

Our original proposal estimated 1100 targets available. The program was allocated 300 targets for entry into the whole gap-filler coordinate pool[4], so much of the time available for detailed preparation went into winnowing the target list. Sparse categories (in practice, those with fewer than 10 examples) were carried along "as is".

Because of the public-participation nature of the Galaxy Zoo projects, and further encouraged by comments from STScI, we solicited public input to select the objects to be listed from categories with a large enough number of galaxies. After members of the science team inspected them for suitability, we set up a web-based voting system, and advertised this opportunity widely through each project's Web and social-media presence, and coordinated with the STScI social-media team for announcement through their accounts as well. We used the Zooniverse Project Builder interface[5] (Trouille et al. 2019), producing parallel selection interfaces for the Galaxy Zoo and Radio Galaxy Zoo subsets. The voting was open from 2-18 February 2018, to meet the 28 February deadline for submission of the Phase 2 proposal with target names, coordinates, and observation details. The Galaxy Zoo categories drew 6199 votes among 292 galaxies (mean 21.2 per object), while the Radio Galaxy Zoo objects attracted 9730 votes among 286 galaxies (mean 34.0 each). Numbers of votes per object varied as users did different numbers per session. The Project Builder interface was set up so that volunteers would cycle through all members of each science category in sequence, with the option to see a montage of available objects in that category to allow a more informed comparative ranking. As illustrated in Fig. 1, each was presented with a question of the form "What priority would you give this galaxy with an unusual spiral pattern for possible Hubble Space Telescope observations?" and possible answers lowest priority, low, medium priority, high, or highest priority.

In collating votes, we could distinguish between users who signed in with a Zooniverse account and those participating anonymously. For the former, registered users, we could recognize multiple votes for a single object, and counted only the last one. We examined the anonymous votes for any evidence of such misbehavior as robotic software packing votes, which could affect the outcome. There were very few anonymous votes (180 for Galaxy Zoo, 247 for Radio

---

[4] One later became impossible to schedule after tighter restrictions became necessary on guide-star flux.

[5] https://www.zooniverse.org/lab
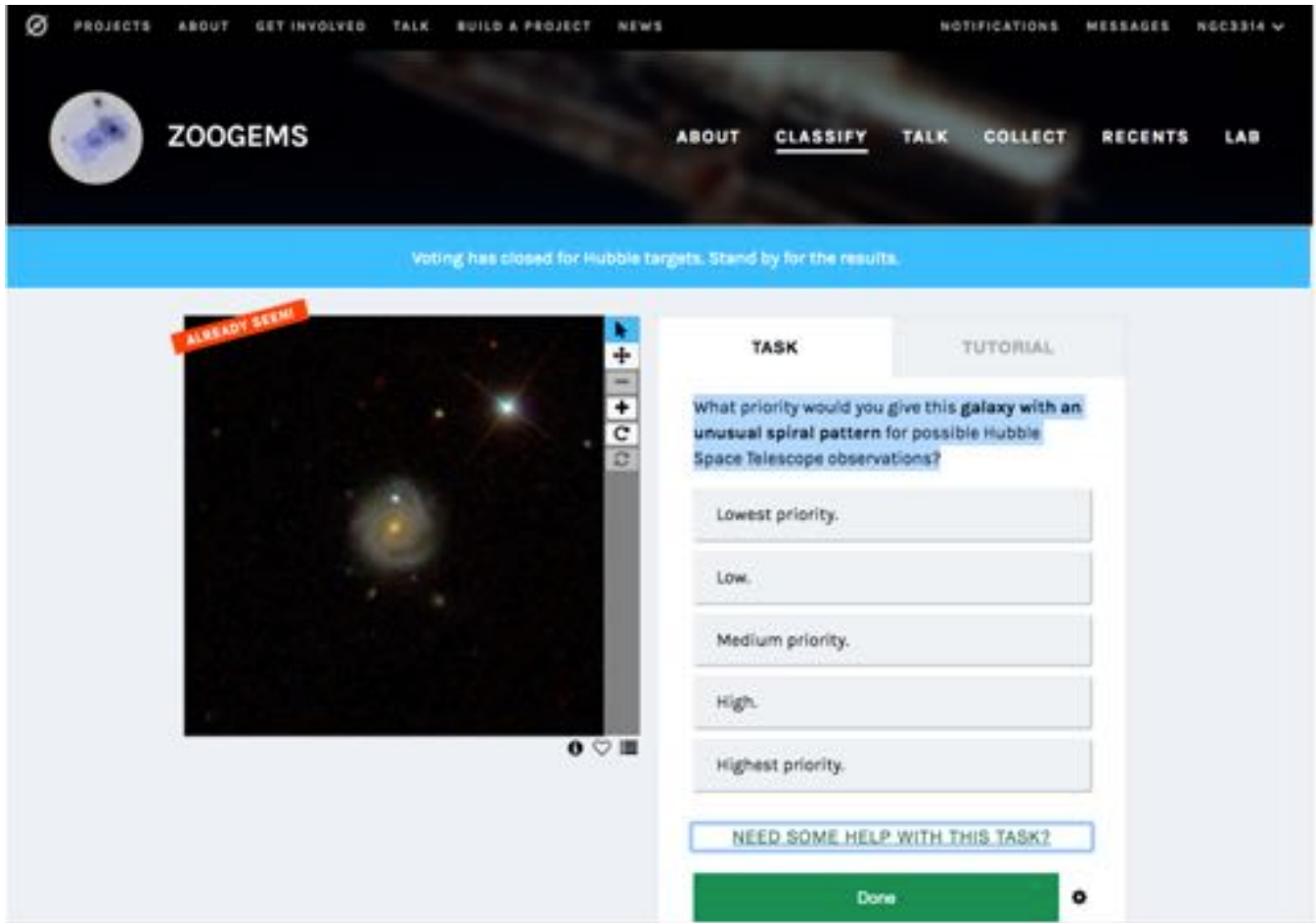
Figure 1. Screen capture of the voting interface for Galaxy Zoo targets. Clicking on "Need some help with this task?" displayed a longer description and a montage of all galaxies in the same voting category. The red banner at upper left indicates that a user has already seen this object.

Galaxy Zoo), widely spread across galaxies, so we saw no evidence of problematic behavior and included these votes in our rankings. Within each science category being voted on, we ranked objects using a straightforward mean of votes weighted by priority. Users were given a 5-point scale to select on seeing each galaxy image; we ranked on the mean with highest priority=1, lowest priority=5. The highest-ranked objects in each science category were carried into the final target list . (The number of slots allocated for each science category was arbitrarily set by the PI, attempting to reflect the number of input objects and scientific interest).

The preliminary target list was shared for discussion with the Galaxy Zoo community on the Talk interface. Volunteers identified some duplicates, because objects could enter in different science categories by different names. We also coordinated our target list with that of gap-filler program 15446 (Arp and Arp-Madore interacting galaxies, P.I. Julianne Dalcanton), to eliminate duplications while ensuring that some especially interesting systems were on one list or the other.

For Green Peas, whose unresolved SDSS images made visual selection superfluous, the input list consisted of SDSS DR12 objects with secure matches to the Portsmouth spectral fitting catalog (Thomas et al. 2013), and BPT type "Star Forming" from that catalog. Further selection was for the brightest objects in each of three redshift ranges where ACS filters (mostly) isolate continuum.
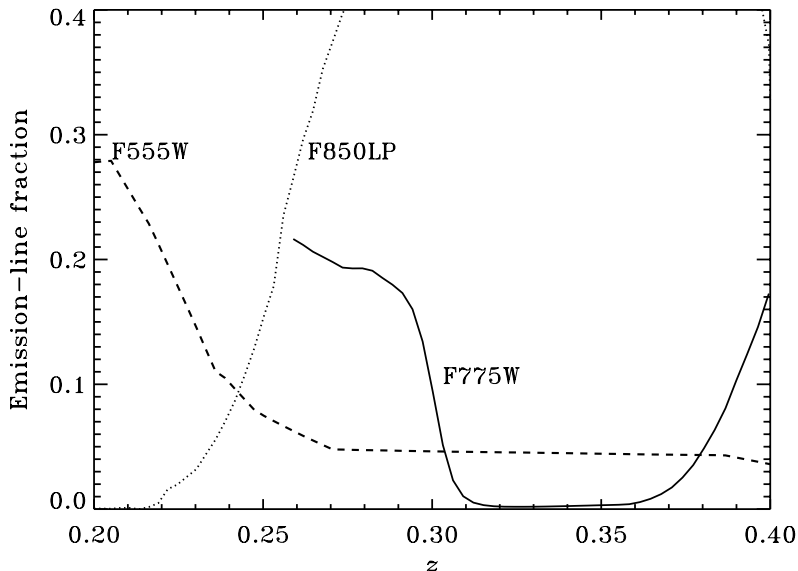
Figure 2. Emission-line contribution in the F555W, F775W, and F850LP passbands for a typical Green Pea spectrum, SDSS J131036.73+214817.0 at $z = 0.2832$, evaluated at various redshifts, showing the range near $z = 0.24$ where both the very broad F555W and F850LP filters have $< 10\%$ contribution from emission lines, and the very deep minimum in the F775W filter from $z = 0.32 - 0.36$ where the contamination from line emission is well below 1%.

Our category for each targeted object was entered in the phase 2 proposal file[6] under the "Comments" field.

Some of the flavor of the voting outcomes can be seen in Fig. 3, showing the top-ranked galaxies in four categories with numerous objects examined.

Table 1 lists the number of target objects in each category, and the number observed as of submission of this paper. Only primary categories are given, although some fit in multiple categories. For example, all five of the Galaxy Zoo EELR systems occur in interacting galaxies, and one Radio Galaxy Zoo lens candidate lies in the same ACS field as the Galaxy Zoo EELR candidate SDSS J160646.74+565139.2. For categories where targets were selected by voting, the table also lists the number of objects voted on in each category and the number of votes received. "Number input" is the number of targets from that category included in the final observing list, and "Observed" is the number actually observed to date.

## 4. OBSERVATION SETUP

The gap-filler proposal category originated with the realization within STScI that there were schedule gaps too short for typical snapshot programs, so that the observational output of HST could be further enhanced by programs with large target lists, ideally spread around the sky or at least around all right ascensions, which could make effective use of short observation windows. This rationale, and the review process for gap-filler programs, are described by MacKenty (2017). Use of the Wide-Field Camera (WFC) mode of the Advanced Camera for Surveys (ACS; Ford et al. 1998) was mandated for gap-filler observations, because of its larger field of view than the Wide Field Camera 3 (WFC3), and to minimize use of a moving mirror in WFC3 identified as a potential failure mode.

An internal STScI pilot project (program 14840) observed bright NGC galaxies, using pairs of 337-second exposures with short dither motions in between. All three gap-filler programs finally scheduled use these same exposure

---

[6] Available at https://www.stsci.edu/hst/phase2-public/15445.pdf
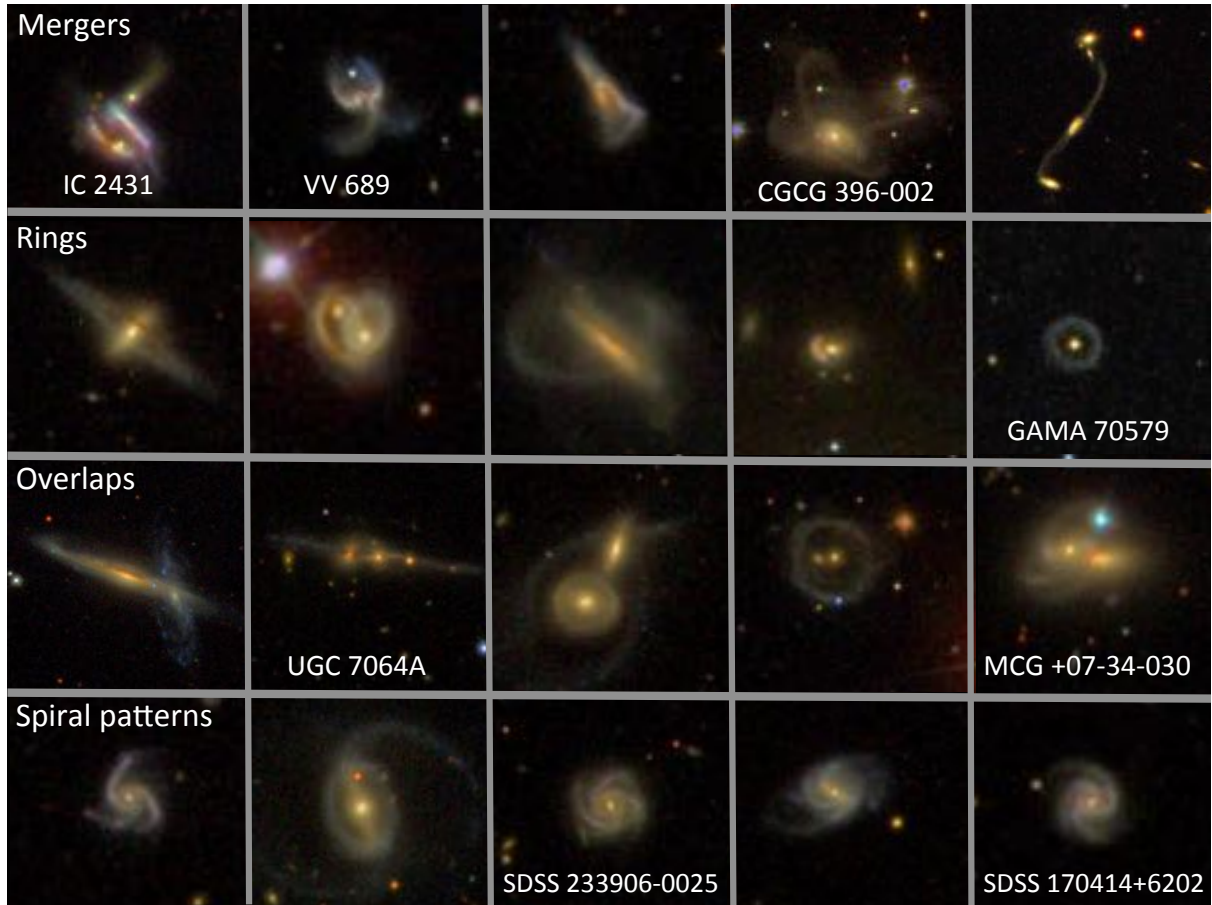
Figure 3. Montage of SDSS gri images of galaxies highest-ranked in the voting among four large categories. Object names are shown for those which have been observed at the time of submission.

times, since the pilot program had demonstrated that there were a significant number of schedule gaps which could accommodate this sequence after guide-star acquisition.

Having settled on the exposure strategy for each object, the available choices were filter, dither strategy, target location in the ACS field, and (in a few cases among Green Peas) whether to do 2 dithered exposures or one exposure each in two filters. The filter selection followed the science goal - if we were interested mostly in spiral structure, the bluer F475W (roughly SDSS g) filter was chosen to enhance its contrast. If the goal was bulge structure, its signal-to-noise ratio would be best in the F814W filter. When the goal was emission-line structure already identified in the SDSS r filter, we used the closely-matching F625W filter. The filter choices and rationale for each object category are listed in Table 1.

For Green Pea systems, our aim was to study the continuum structure, using filters dominated by the stellar population rather than ionized gas. We were guided by the results of numerically redshifting a typical Pea spectrum and folding through the system response for several filters (Fig. 2) . For 35 Green Peas in the redshift range $z = 0.32 - 0.36$, we used the F775W filter, with emission-line fraction $< 0.3\%$. For Green Peas near $z = 0.15$ (12 objects), we used F850LP where that is dominated by continuum, while for the 27 targets near $z = 0.25$, we took single exposures in F555W and F850LP which are each mostly continuum, tolerating the numerous cosmic-ray events since the targets are small. Except for this small number of two-filter Green Pea observations, we used a common two-point dither pattern designed to fill the chip gap (albeit with a central band of cosmic-ray features resulting from coverage with only one exposure in this area).

Table 1. Target and Filter selection by Object Categories

Category	Number voted	Votes	Number Input	Observed	Filter	Goal
Galaxy Zoo ring systems	26	799	15	6	F606W	Overall structure
Galaxy Zoo EELRs	—	—	5	1	F475W	Line emission
Galaxy Zoo regrowing disks	—	—	7	6	F606W	Overall structure
Galaxy Zoo bulges	—	—	9	5	F814W	Old populations
Galaxy Zoo interacting systems	15	515	10	7	606W	Overall structure
Galaxy Zoo red/blue pairs	—	—	5	2	F606W	Overall structure
Galaxy Zoo star-forming clumps	36	904	7	1	F606W	Overall structure
Galaxy Zoo spiral patterns	17	490	7	4	F475W	Young populations
Galaxy Zoo poststarbursts	56	1396	20	5	F475W	Young clusters
Galaxy Zoo overlapping pairs	63	1566	21	7	F606W	Dust structure
Galaxy Zoo nuclear disks/bars	—	—	8	4	F814W	Old populations
Galaxy Zoo blue ellipticals	61	1569	12	6	F475W	Spiral structure
Galaxy Zoo red spirals	19	517	5	1	F606W	Overall structure
Galaxy Zoo Green Peas: all	—	—	74	38		Stellar continuum
Green Peas: single filter	—	—	47	23	F775W	Stellar continuum
Green Peas: 2 filters	—	—	27	15	F555W+F850LP	Stellar continuum
Radio Galaxy Zoo SDRAGNs	214	7110	65	32	F475W	Spiral structure
Radio Galaxy Zoo EELRs	72	2620	36	18	F625W	Line emission

Target locations on the ACS chips were set in view of the charge-transfer trailing occurring in these CCDs. While the effects can be substantially reduced with the pixel-based algorithm, essentially a deconvolution, by Anderson & Bedin (2010), the effect is reduced in the first place if the number of charge transfers can be minimized by placing the target close to the readout amplifier. Since orientation had to be unconstrained for snapshot observations, we identified a circular region of interest for each target, including the SDSS extent of the galaxy and any nearby obvious companions, and used the interactive ALADIN viewing feature of the Astronomers' Proposal Tool (APT) to define a POS TARG coordinate offset, so that circular region closely abutted the edge of CCD WFC1. We considered putting targets closer to the corner of the overall ACS WFC field where optical distortion gives the largest pixels on the sky, in order to improve surface-brightness sensitivity, but that region falls on CCD WFC2 whose slightly higher readout noise more than compensates for the pixel-area difference in sensitivity.

During this stage, we also caught some pasting errors in the sign of target declinations, possibly fostered by having target lists and formats from multiple sources.

5. SAMPLE RESULTS

The Zoo Gems observations to date are listed in Table 2, by science topic and observation date. As of 31 January 2022, 146 objects had been observed, 49% of the input list. The total exposure time in each case is 674 seconds, in two dithered exposures when a single filter was used, or two individual 337-second exposure for those Green Peas with two filters listed. For these 2-filter objects, we list the final two characters of the second data set identifier after the complete identifier for the first exposure. In a few cases, one exposure was terminated onboard before the planned duration.

The ACS images showed some objects to be morphologically rather different than we anticipated from SDSS images. In these cases, we show them in Table 2 and in our further discussion according to the category where they fit most closely rather than the category listed in the proposal. One object, SDSS J222024.58+010931.3, turned out to be a superposition of a star and faint background galaxies which mimicked a ring structure in the SDSS data, and is not included in Table 2.

The following sections highlight some initial results from the Zoo Gems observations, and demonstrate the value of even such shallow exposures in addressing a variety of scientific questions.

Table 2. Zoo Gems Observations

Dataset	Target Name	α_{2000}	δ_{2000}	UT Start Time	Filter
Unusual spiral patterns:					
JDS452010	SDSS-170414.33+620234.0	17 04 16.225	+62 02 57.91	2018-07-06 08:19:20	F475W
JDS450010	UGC-4250	08 10 05.486	+46 11 34.90	2021-01-11 05:23:05	F475W
JDS451010	NGC-2595	08 27 42.024	+21 28 44.76	2021-03-16 11:57:55	F475W
JDS453010	MCG+10-21-019	14 36 35.851	+57 47 49.08	2021-08-03 20:07:36	F475W
JDS454010	SDSS-233906.23-002615.0	23 39 06.236	-00 26 15.10	2021-11-13 12:36:39	F475W
X-Bulges:					
JDS439010	NGC-1175	03 04 30.752	+42 20 07.55	2019-07-18 02:34:29	F814W
JDS436010	SDSS-1237661418212229211	14 09 04.333	+54 52 19.88	2019-09-07 11:43:00	F814W
Nuclear disks/bars:					
JDS498010	CGCG-245-033	13 12 56.707	+47 27 23.84	2021-03-12 22:49:26	F814W
JDS40A010	NGC-2771	09 10 41.192	+50 22 36.54	2021-03-14 01:09:33	F814W
JDS40B010	NGC-5945	15 29 45.007	+42 55 07.13	2021-03-14 04:40:37	F814W
JDS40F010	MCG+09-19-030	11 17 43.510	+53 47 36.25	2021-09-27 04:08:05	F814W
Large or prolate bulges:					
JDS420010	NGC-0810	02 05 28.560	+13 15 05.76	2019-06-24 18:54:23	F606W
JDS435010	CGCG-308-012	06 13 05.304	+64 33 41.04	2019-12-19 07:05:33	F814W
JDS47T010	UGC-10374	16 23 39.166	+50 58 09.96	2020-03-03 13:11:57	F814W
Red/Blue Pairs:					
JDS432010	SDSS-1237678618479755694	22 12 06.397	+01 46 06.37	2019-11-28 19:29:10	F606W
JDS431010	GAMA-636444	09 23 21.888	-01 43 33.96	2022-01-29 18:48:26	F606W
Star-forming knots:					
JDS430010	GAMA-302130	09 05 46.392	+01 15 32.76	2021-10-06 04:06:12	F606W
Overlapping Galaxies:					
JDS437010	SDSS-1237661417676800323	14 28 14.096	+53 14 29.00	2019-05-08 08:33:55	F814W
JDS490010	SDSS-115331.86+360024.2	11 53 31.865	+36 00 24.27	2019-05-28 18:56:44	F606W
JDS478010	UGC-7064A	12 04 44.973	+60 40 24.56	2019-07-12 11:33:01	F606W
JDS488010	NGC-5021	13 12 06.265	+46 11 45.75	2020-07-16 12:05:54	F814W
JDS489010	UGC-12281	22 59 14.839	+13 36 16.74	2020-09-01 04:48:39	F606W
JDS485010	IC-720	11 42 22.336	+08 46 11.51	2021-03-14 06:10:29	F606W
JDS481010	MCG+07-34-030	16 25 58.133	+43 57 46.47	2021-10-10 11:32:38	F606W
Interacting/Merging Systems:					
JDS449010	SDSS-081913.94+591926.4	08 19 13.920	+59 19 26.76	2019-02-22 21:23:13	F606W
JDS47W010	UGC-00240	00 25 10.106	+06 29 27.17	2019-10-05 06:19:39	F606W
JDS44M010	VII-ZW-090	10 36 35.625	+02 21 31.41	2020-02-27 03:33:10	F475W
JDS428010	SDSS-095346.77-012746.1	09 53 46.680	-01 27 45.00	2020-03-03 05:50:45	F606W
JDS406010	SDSS-1237668504364187727	16 12 24.606	+59 46 10.47	2021-03-14 03:53:56	F475W
JDS444010	CGCG-396-002	05 37 35.976	+01 20 04.20	2021-03-18 22:36:26	F606W
JDS442010	VV-689	10 01 39.502	+19 47 32.58	2021-04-30 17:06:39	F606W
JDS441010	IC-2431	09 04 34.776	+14 35 45.96	2021-10-03 02:54:35	F606W
Ring(ed) Galaxies, Lenses:					
JDS425010	SDSS-1237679438812676365	02 03 28.727	-06 59 49.72	2019-02-17 01:28:33	F606W

Table 2 *(continued)*

Dataset	Target Name	α_{2000}	δ_{2000}	UT Start Time	Filter
JDS426010	CGCG-087-009	07 33 17.712	+18 17 24.36	2019-03-20 14:17:24	F606W
JDS418010	GAMA70579	12 01 43.464	+00 10 59.16	2019-05-17 06:34:36	F606W
JDS424010	SDSS-133145.32+513431.2	13 31 45.326	+51 34 31.22	2019-09-08 17:53:10	F814W
JDS495010	IC-3828	12 50 20.695	+37 56 56.19	2020-06-13 17:27:34	F606W
JDS405010	SDSS-1237678595932094536	22 20 24.589	+01 09 31.30 0	2020-12-16 21:52:36	F475W
JDS427010	SDSS-081740.08+042952.3	08 17 40.080	+04 29 52.44 0	2021-01-12 21:07:04	F606W
Galaxy Zoo EELRs:					
JDS403010	SDSSJ160646.74+565139.2	16 06 46.740	+56 51 39.20	2021-12-24 16:13:14	F606W
Radio Galaxy Zoo EELRs:					
JDS46N010	SDSS-130854.52+562155.6	13 08 52.460	+56 22 42.40	2019-02-15 02:12:01	F625W
JDS46Z010	SDSS-075529.95+520450.6	07 55 26.309	+52 03 51.25	2019-04-02 07:46:09	F625W
JDS46U010	SDSS-102733.29+544227.9	10 27 30.688	+54 41 30.79	2019-06-04 03:47:14	F625W
JDS46R010	SDSS-121849.88+502617.6	12 18 45.908	+50 25 30.87	2019-06-07 00:40:21	F625W
JDS46E010	SDSS-160344.95+524220.6	16 03 42.715	+52 41 25.34	2019-08-20 14:58:52	F625W
JDS47M010	SDSS-010206.98+093427.6	01 02 03.668	+09 35 04.12	2019-10-08 21:44:09	F625W
JDS47G010	PKS-0236+02	02 38 34.584	+02 34 46.84	2019-10-16 03:00:46	F625W
JDS47V010	SDSS-101147.31+071915.2	10 11 50.739	+07 19 42.52	2020-02-15 07:07:13	F625W
JDS46H010	SDSS-025210.17+025430.1	02 52 10.017	+02 53 32.90	2020-03-06 11:15:15	F625W
JDS47C010	SDSS-141119.04+094225.3	14 11 19.04	+09 42 25.3	2020-08-02 17:12:10	F625W
JDS46I010	SDSS-105426.23+573649.1	10 54 32.316	+57 37 16.16	2020-10-17 09:26:49	F625W
JDS47F010	SDSS-082400.50+031749.4	08 24 04.353	+03 18 07.73	2021-01-14 06:29:16	F625W
JDS46C010	B2-0832+34	08 35 15.391	+34 34 01.90	2021-03-12 06:17:49	F625W
JDS46W010	SDSS-083512.43+175441.0	08 35 10.668	+17 53 50.09	2021-03-19 01:55:27	F625W
JDS47D010	SDSS-123300.30+060326.1	12 32 58.539	+06 04 16.38	2021-03-21 08:13:26	F625W
JDS46P010	3C-458	23 12 48.445	+05 17 05.36	2021-09-10 03:03:35	F625W
JDS46Q010	4C+08.70	23 36 40.401	+08 49 55.09	2021-09-12 04:19:16	F625W
JDS46O010	SDSS-141408.44+484156.0	14 14 08.445	+48 41 56.00	2021-09-22 01:59:54	F625W
Blue Elliptical Galaxies:					
JDS40O010	CGCG-315-014	12 06 17.055	+63 38 19.08	2019-04-15 14:34:09	F475W
JDS40M010	MKN-0888	16 44 30.755	+19 56 26.73	2019-08-07 09:15:53	F475W
JDS40P010	SDSS-111850.04+422541.8	11 18 50.047	+42 25 41.84	2019-12-28 23:11:30	F475W
JDS40H010	SDSS-031749.30+011337.1	03 17 49.304	+01 13 37.25	2020-11-28 06:10:32	F475W
JDS40J010	SDSS-000907.90+142755.8	00 09 07.908	+14 27 55.83	2021-08-06 09:06:11	F475W
JDS40G010	CGCG-432-030	23 47 03.791	+14 50 30.36	2021-09-17 06:36:51	F475W
Red spiral galaxies:					
JDS40T010	UGC 3935	07 37 49.410	+46 23 51.53	2020-10-18 00:25:12	F606W
Regrowing-disk Mergers:					
JDS414010	NGC-2292	06 47 40.830	-26 45 05.00	2020-01-23 04:22:48	F606W
JDS412010	CFHTLS1220-215555	08 50 58.169	-04 02 12.85	2020-03-12 02:41:03	F606W
JDS410010	UGC-4052	07 51 16.564	+50 14 03.27	2020-05-01 11:33:05	F606W
JDS408010	SDSS-1237659369978568047	00 43 41.784	+43 02 35.16	2020-12-19 19:47:02	F606W
JDS413010	SDSS-1237680246274064522	23 26 23.853	+19 27 09.12	2021-09-20 01:17:10	F606W
JDS409010	SDSS-1237678439701807265	02 49 03.312	+03 12 12.60	2021-09-21 09:16:29	F606W

Table 2 *(continued)*

| Dataset	Target Name	α_{2000}	δ_{2000}	UT Start Time	Filter
Post-Starburst Galaxies:					
JDS464010	CGCG-292-024	11 44 52.092	+57 52 24.67	2018-08-09 03:21:12	F475W
JDS474010	SDSS-124354.11+163250.5	12 43 54.178	+16 32 50.85	2019-03-19 13:30:53	F475W
JDS460010	NGC-3156	10 12 41.183	+03 08 04.71	2020-02-24 16:44:52	F475W
JDS457010	UGCA-188	09 55 29.700	+08 23 26.28	2020-06-12 20:44:08	F475W
JDS476010	VCC-1711	12 37 22.147	+12 17 13.32	2021-03-21 19:20:48	F475W
SDRAGNs:					
JDS45H010	SDSS-091949.07+135910.7	09 19 47.195	+13 58 22.68	2018-05-15 21:49:55	F475W
JDS43Y010	UGC-1797	02 19 58.728	+01 55 48.72	2018-07-03 02:46:37	F475W
JDS44C010	SDSS-16562058+6407529	16 56 16.945	+64 07 14.62	2018-08-24 13:52:36	F475W
JDS45T010	SDSS-112811.63+241746.9	11 28 09.853	+24 18 39.94	2019-02-23 05:51:12	F475W
JDS45Z010	B3-1352+471	13 54 30.924	+46 56 44.51	2019-04-28 00:35:49	F475W
JDS44X010	SDSS-132809.31+571023.3	13 28 03.443	+57 10 13.25	2019-05-14 07:06:26	F475W
JDS45J010	SDSS-163300.85+084736.4	16 32 58.024	+08 47 03.84	2019-07-11 23:11:15	F475W
JDS44Z010	B2-1644+38	16 46 25.987	+38 31 03.31	2019-07-19 17:39:53	F475W
JDS43V010	SDSS-172107.89+262432.1	17 21 05.558	+26 23 54.34	2019-08-22 16:18:28	F475W
JDS47J010	SDSS-134900.13+454256.5	13 49 06.051	+45 43 03.52	2019-11-13 21:02:54	F475W
JDS45V010	SDSS-214110.61+082132.6	21 41 11.564	+08 20 35.91	2019-12-11 14:04:35	F475W
JDS45G010	SDSS-081303.10+552050.7	08 13 00.417	+55 21 37.26	2019-12-25 01:19:10	F475W
JDS44D010	SDSS-150903.21+515247.9	15 09 08.415	+51 53 28.37	2020-01-14 13:19:06	F475W
JDS44R010	B2-0938+31A	09 40 59.773	+31 26 29.12	2020-02-13 02:39:49	F475W
JDS47H010	SDSS-095605.87+162829.9	09 56 01.712	+16 28 52.37	2020-02-14 21:34:14	F475W
JDS45A010	IC-4234	13 22 58.535	+27 07 09.45	2020-04-09 03:03:16	F475W
JDS44J010	SDSS-080658.46+062453.4	08 06 58.46	+06 24 53.4	2020-05-28 23:07:53	F475W
JDS44P010	SDSS-095833.44+561937.8	09 58 39.333	+56 20 16.06	2020-10-17 13:19:01	F475W
JDS44I010	SDSS-080259.73+115709.7	08 03 04.152	+11 57 33.22	2021-01-10 03:57:52	F475W
JDS47K010	SDSS-113648.57+125239.7	11 36 48.57	+12 52 39.7	2021-03-14 02:58:57	F475W
JDS41L010	B3-0852+422	08 55 44.151	+42 03 44.70	2021-03-14 23:24:25	F475W
JDS45L010	SDSS-090305.84+432820.4	09 03 02.290	+43 27 51.56	2021-03-15 00:59:46	F475W
JDS44G010	SDSS-082312.91+033301.3	08 23 11.663	+03 32 03.79	2021-03-15 05:49:08	F475W
JDS45B010	SDSS-083351.28+045745.4	08 33 50.118	+04 56 54.67	2021-03-18 00:32:22	F475W
JDS45F010	SDSS-163624.97+243230.8	16 36 21.753	+24 32 46.26	2021-06-05 19:19:04	F475W
JDS44K010	SDSS-083224.82+184855.4	08 32 27.328	+18 49 54.04	2021-09-28 05:30:40	F475W
JDS45E010	SDSS-130300.80+511954.7	13 03 00.803	+51 19 54.70	2021-10-01 05:04:08	F475W
JDS45I010	SDSS-084759.90+124159.3	08 47 59.90	+12 41 59.3	2021-10-02 04:44:49	F475W
JDS44T010	SDSS-020904.75+075004.5	02 09 04.750	+07 50 04.50	2021-10-22 03:54:22	F475W
JDS45W010	SDSS-090147.17+164851.3	09 01 47.17	+16 48 51.3	2021-11-13 10:05:19	F475W
JDS43Z010	B3-0911+418	09 14 45.528	+41 37 14.52	2021-12-29 08:17:30	F475W
JDS47L010	SDSS-092605.17+465233.9	09 26 05.17	+46 52 33.9	2021-12-29 19:23:05	F475W
Green Peas:					
JDS42MO4Q/5Q	SDSS-1237651537646977181	15 04 57.987	+59 54 07.27	2018-07-10 14:11:15	F555W, F850LP
JDS42KCEQ/FQ	SDSS-1237659330316140926	16 33 37.941	+37 53 14.30	2018-07-14 03:38:45	F555W, F850LP

Table 2 *(continued)*

Dataset	Target Name	α_{2000}	δ_{2000}	UT Start Time	Filter
JDS41D010	SDSS-1237648720155902209	11 49 46.471	-01 02 17.65	2018-11-29 21:59:41	F775W
JDS41F010	SDSS-1237661386530882021	14 10 05.248	+53 50 37.89	2018-12-27 01:56:41	F775W
JDS40X010	SDSS-1237651271358349509	10 26 15.207	+63 33 08.49	2019-01-02 02:51:41	F775W
JDS40Y010	SDSS-1237657878078751164	08 08 16.907	+28 14 31.14	2019-02-24 00:38:23	F775W
JDS42IUGQ/HQ	SDSS-1237654398623023110	13 36 07.914	+62 55 30.77	2019-04-12 02:35:01	F555W, F850LP
JDS40Z010	SDSS-1237651271899939173	12 05 17.538	+66 40 29.64	2019-04-19 05:30:54	F775W
JDS42ZV5Q/6Q	SDSS-1237667551414452597	10 15 41.152	+22 27 27.52	2019-05-16 16:09:08	F555W, F850LP
JDS42QJPQ/QQ	SDSS-1237661851469021323	12 14 23.180	+45 20 40.91	2019-07-17 04:52:31	F555W, F850LP
JDS42B010	SDSS-1237669698364768508	21 08 03.059	+05 27 07.14	2019-08-10 04:15:11	F775W
JDS41A010	SDSS-1237651273498755389	08 38 40.165	+54 44 03.49	2019-10-01 17:20:01	F775W
JDS43DUMQ/NQ	SDSS-1237666300559098162	03 53 32.464	-00 10 28.88	2019-11-14 06:16:30	F555W, F850LP
JDS42F010	SDSS-1237680507722793618	23 19 27.467	+33 23 24.76	2019-11-25 15:15:51	F775W
JDS43EDKQ/LQ	SDSS-1237665369575981438	10 20 57.462	+29 37 26.47	2020-01-26 23:25:54	F555W, F850LP
JDS42WWCQ/DQ	SDSS-1237667536933945523	10 04 00.641	+20 17 19.25	2020-02-21 03:03:38	F555W, F850LP
JDS43T010	SDSS-1237664668421849521	08 15 52.002	+21 56 23.65	2020-04-27 20:20:00	F850LP
JDS42LSNQ/OQ	SDSS-1237658491735507237	10 55 30.41	+08 41 32.8	2020-06-03 14:22:26	F555W, F850LP
JDS43M010	SDSS-1237657632187613477	09 24 38.718	+47 07 58.93	2020-06-10 20:58:36	F850LP
JDS41Q010	SDSS-1237662300818702524	13 01 28.316	+51 04 51.18	2020-08-01 18:46:22	F775W
JDS42NVWQ/XQ	SDSS-1237653653450064110	00 42 36.92	+16 02 02.7	2020-11-12 16:48:32	F555W, F850LP
JDS42HVJQ/KQ	SDSS-1237660343930782057	08 45 11.669	+32 51 53.92	2020-12-09 06:05:51	F555W, F850LP
JDS41G010	SDSS-1237654383585395027	08 34 40.056	+48 05 40.91	2021-01-11 21:16:54	F775W
JDS42E010	SDSS-1237667254538142046	09 51 03.165	+24 54 35.70	2021-02-07 10:29:06	F775W
JDS42XQMQ/NQ	SDSS-1237667211050680599	09 41 49.637	+23 37 30.07	2021-02-14 12:28:58	F555W, F850LP
JDS41U010	SDSS-1237662640662905610	16 46 12.15	+20 54 11.5	2021-03-13 05:34:25	F775W
JDS43J010	SDSS-1237658423543529721	09 05 35.161	+04 53 34.51	2021-03-18 02:09:30	F850LP
JDS42SAJQ/KQ	SDSS-1237648704041976118	12 29 33.142	-00 18 01.68	2021-03-26 05:48:14	F555W, F850LP
JDS42UHCQ/DQ	SDSS-1237667781210145026	10 04 34.733	+17 47 35.35	2021-04-27 00:09:42	F555W, F850LP
JDS43CVFQ/GQ	SDSS-1237679476939882858	01 03 21.059	+21 32 15.91	2021-09-09 17:36:16	F555W, F850LP
JDS43N010	SDSS-1237655373039927410	16 53 04.490	+33 39 37.74	2021-09-09 18:57:15	F850LP
JDS43O010	SDSS-1237663782590021909	00 29 38.169	-01 12 16.05	2021-09-17 05:07:19	F850LP
JDS41R010	SDSS-1237657589239382254	09 54 22.599	+47 51 44.02	2021-09-22 03:22:49	F775W
JDS41S010	SDSS-1237661382770098472	09 20 36.046	+32 42 52.63	2021-09-29 03:39:51	F775W
JDS41J010	SDSS-1237663204918952341	00 44 00.266	+00 47 24.68	2021-09-30 23:56:42	F775W
JDS41I010	SDSS-1237657628456386802	12 33 38.626	+51 41 59.34	2021-10-01 01:52:15	F775W
JDS42JI3Q/4Q	SDSS-1237660635458568341	10 27 16.725	+43 42 02.18	2021-10-03 06:30:17	F555W,F850LP
JDS41P010	SDSS-1237661361304568164	14 46 42.608	+40 48 44.21	2021-12-11 16:35:48	F775W

5.1. *Green Peas*

The great majority of Green Peas (34/38, 89%) are resolved into multiple distinct components or show surrounding non-axisymmetric structure. The structures include double components, tails, and apparent disks. Four systems (SDSS J004236.92+160202.7, SDSS J092438.71+470758.9, SDSS J100400.64+201719.2, and SDSS J165304.48+333937.7) have central peaks only marginally resolved in the ACS data; a simple Gaussian comparison with star images suggests intrinsic FWHM < 1.8 pixels (0.09″) or 0.36 kpc at the typical $z = 0.25$. Some of the Green Pea systems show tidal
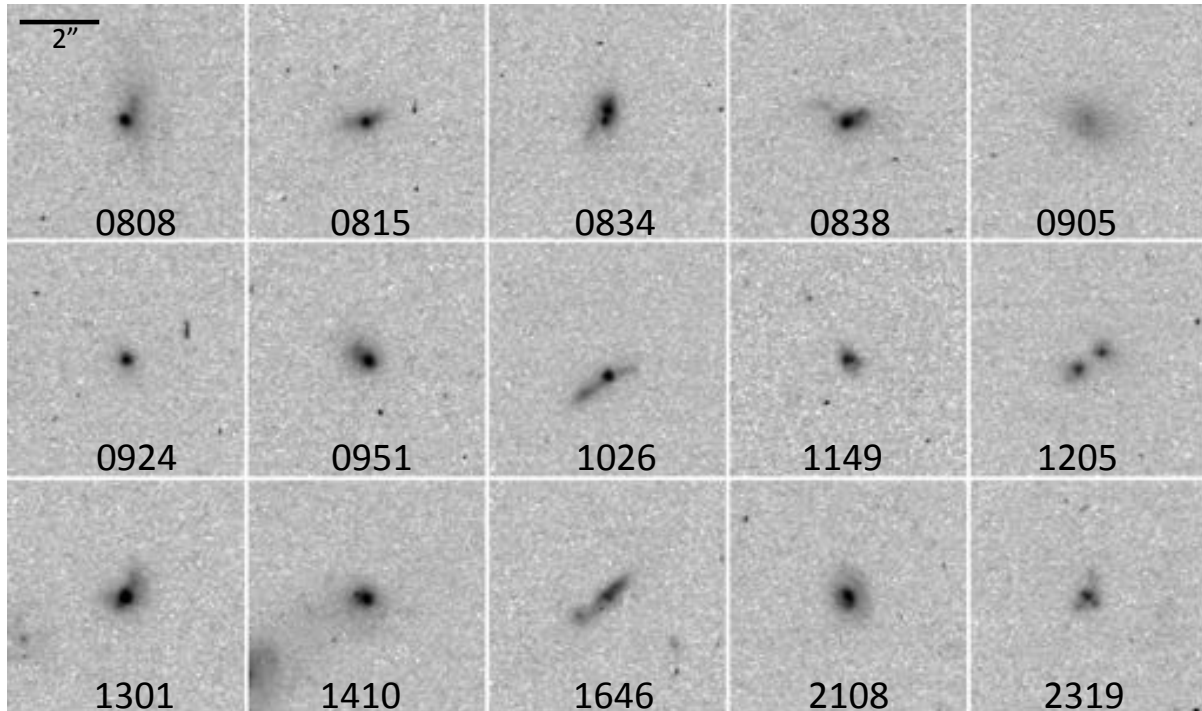
Figure 4. The first 15 Green Pea systems observed in single filters, as listed in Table 2. Abbreviated names showing the first 4 digits of the right ascension are used for convenience. Each panel is a $6 \times 6''$region, typically 24×24 kpc, and all are shown to the same intensity scale, logarithmic above a slight negative offset. North is up, and east to the left in each case. The $2''$scale bar matches the limiting Petrosian radius from SDSS data used in the sample selection. All were observed in the F775M band except 0815, 0905, and 0924, observed in F850LP.

tails or patchy spiral patterns; most have either multiple knots or show well-resolved surrounding galaxies (shown in Fig. 4 for those observed in a single filter, allowing easy rejection of cosmic-ray artifacts). Analysis of the 2-filter Zoo Gems data by Clarke et al. (2020) indicates that the intense starburst regions are surrounded by redder components, most likely older stellar populations. The smallest sizes we measure in these deep-red bands are comparable to the UV sizes measured (predominantly for the brightest components) by Yang et al. (2017) and Kim et al. (2021).

5.2. *Blue ellipticals*

Each of the six blue early-type galaxies observed in Zoo Gems shows a distinct spiral structure, which in each case is too tightly wound to have been resolved in SDSS data (Fig. 5). These are not simply otherwise-normal elliptical galaxies with scattered star-forming regions, although in some cases the outer light distribution is less disc-like than the inner regions. In fact, two of these galaxies, Mkn 888 and SDSS J031749.30+011337, have a nearly pure $r^{1/4}$ profile as assessed in the SDSS *fracDeV* parameter, with values 0.97–1 among all SDSS filters. The other four have values 0.49–0.96 in the well-measured *griz* bands. Among the galaxies observed, SDSS 031749.30+011337.1 and CGCG 432-030 have AGN as classified by Schawinski et al. (2009a) using emission-line ratios from the SDSS spectra. Schawinski et al. (2009b) reported a CO detection of SDSS 111850.04+422541.8, with a double-peaked disk-like profile and implied total molecular-gas mass near 6×10^8 M$_\odot$. These small-scale spiral patterns are similar to those sometimes seen in
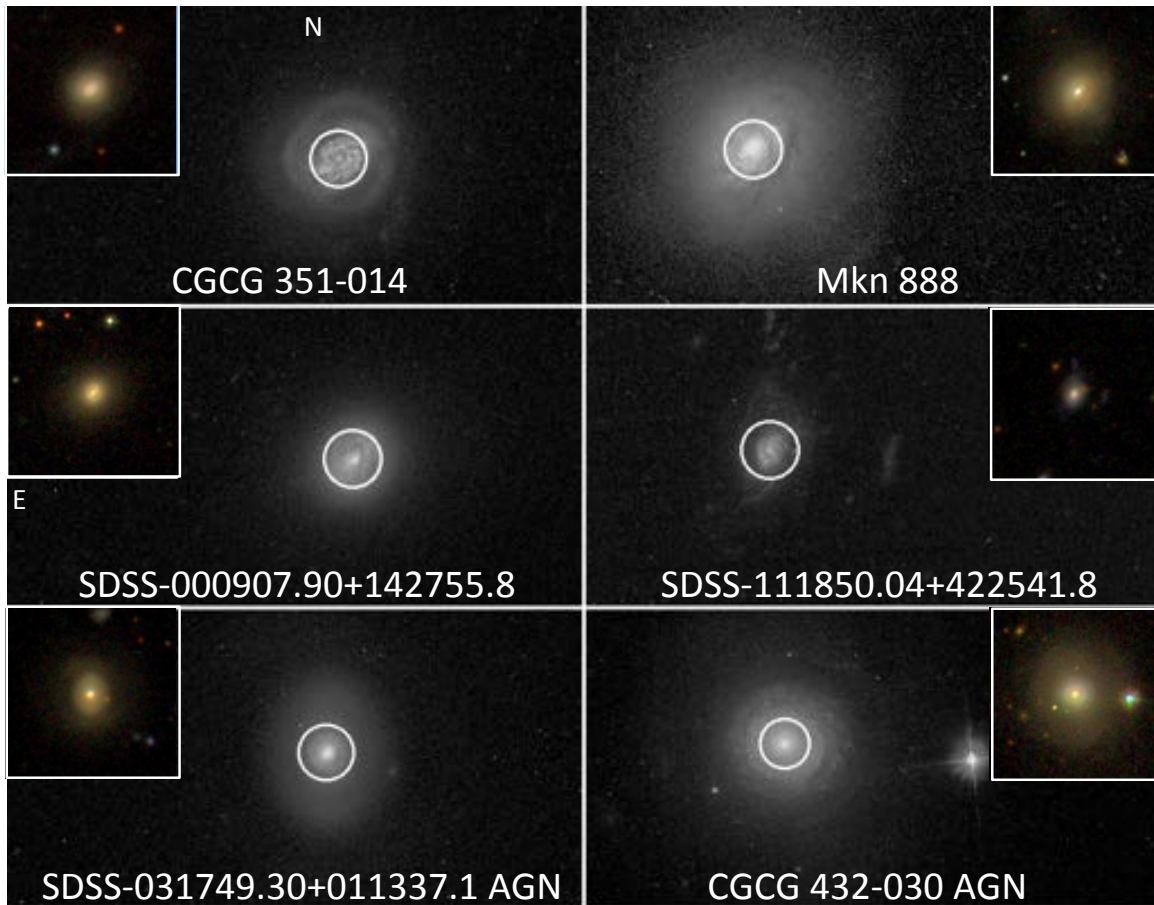
Figure 5. Blue early-type galaxies, in the F475W filter to emphasize young stellar populations. The bottom two are classified as having spectroscopic AGN by the SDSS automated system. Each galaxy shows a tightly wound spiral pattern near the nucleus; the superimposed circles have radius $2.5''$, showing how strongly these patterns are blended together in typical survey images. Insets show SDSS composite images, $60''$square, as used by Galaxy Zoo participants in the initial classifications. Some show various levels of structure in these images, but only CGCG 432-030 might have been classified as a clear spiral from SDSS data. North is up, and east to the left in each case.

recent major mergers, such as NGC 7252 (Whitmore et al. 1993), NGC 3256 (as shown in the figures by Mulia et al. 2016), and even 2MASX J01392400+2924067 seen before coalescence of the nuclei (Koss et al. 2018), which could support the conjecture of Schawinski et al. (2009b) that such mergers are one route to producing blue galaxies with elliptical-like properties. The galaxies in our sample share the radial scales of central spiral patterns with the nearby post-merger systems, as traced both by star clusters and by dust lanes. The dust spirals have radial extents 1.2–3.3 kpc, and the patterns traced by bright star-forming regions span 1.2–2.6 kpc. These are comparable to the values 1.8–6.4 kpc (dust) and 1.2–3.0 kpc (star clusters) seen in nearby merging and post-merger systems. The smaller values apply to NGC 7252, which is the oldest local merger based on comparison with simulations and ages of star clusters, and thus more comparable to our systems where merger signatures in the starlight distribution must be even more subtle.

There is clearly more to be done in defining how these blue early-type galaxies relate to normal ellipticals, mergers, and even rejuvenated spirals. We plan to consolidate these HST images along with the new deep ground-based surveys to address this in future work.

5.3. *Red spirals*

UGC 3935

<div align="center">SDSS gri   HST ACS F606W</div>
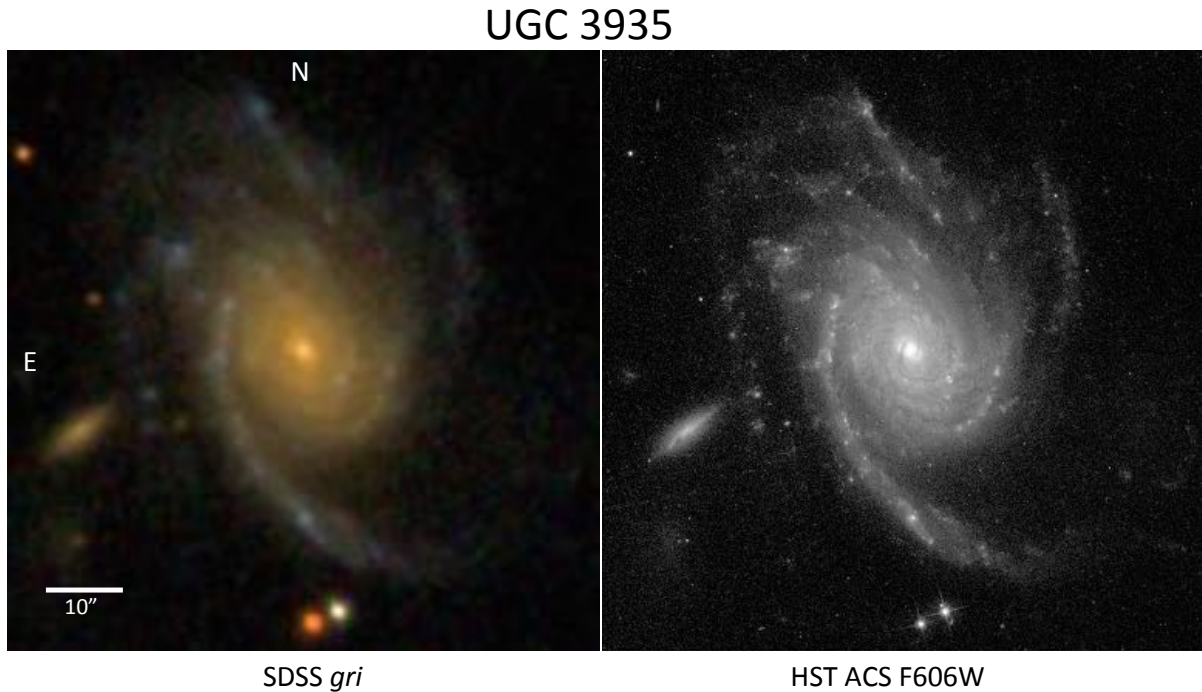
Figure 6. Red spiral galaxy UGC 3935, comparing the usual gri composite from SDSS data with the HST ACS F606W image. The region shown is $77 \times 78''$ with north at the top.

One of these, UGC 3935, has been observed. The arms include star-forming knots, while the dust arms include a spiral pattern cutting across stellar structure near the core. This object was included in the MaNGA survey's integral-field spectroscopy (Bundy et al. 2015), and in the associated and ongoing H I survey (Masters et al. 2019, Stark et al. 2021), which shows 3.7×10^{10} M$_\odot$ of neutral hydrogen. This is close to the derived stellar mass 4.6×10^{10} M$_\odot$ from SDSS data using the Portsmouth models (Maraston et al. 2009), so the galaxy's red color is not due purely to gas exhaustion. The HST image is compared to an SDSS color-composite in Fig. 6. The arms contain blue star-forming knots, and this could be classified as a 3-armed system as well.

5.4. *Disk structures*

The range of disk structures included in Zoo Gems data is sampled in Fig. 7.

5.4.1. *Circumnuclear disks and bars*

The two systems shown in Fig. 7 both have nuclear bars and surrounding rings or barlenses (as defined by Laurikainen et al. 2011), which extend beyond the bar width in each case. The inner region of NGC 2771 forms a striking echo, rotated nearly $90°$, of the outer bar and ring of the galaxy disk. NGC 2595 from the "unusual spiral patterns" category shows similar features. UGC 10374 has an outer pseudoring beyond the area shown. The backlit spiral in IC 720 shows a nuclear spiral and possibly nuclear bar which were not well resolved even in subarcsecond ground-based images.

5.4.2. *Three-armed spirals*
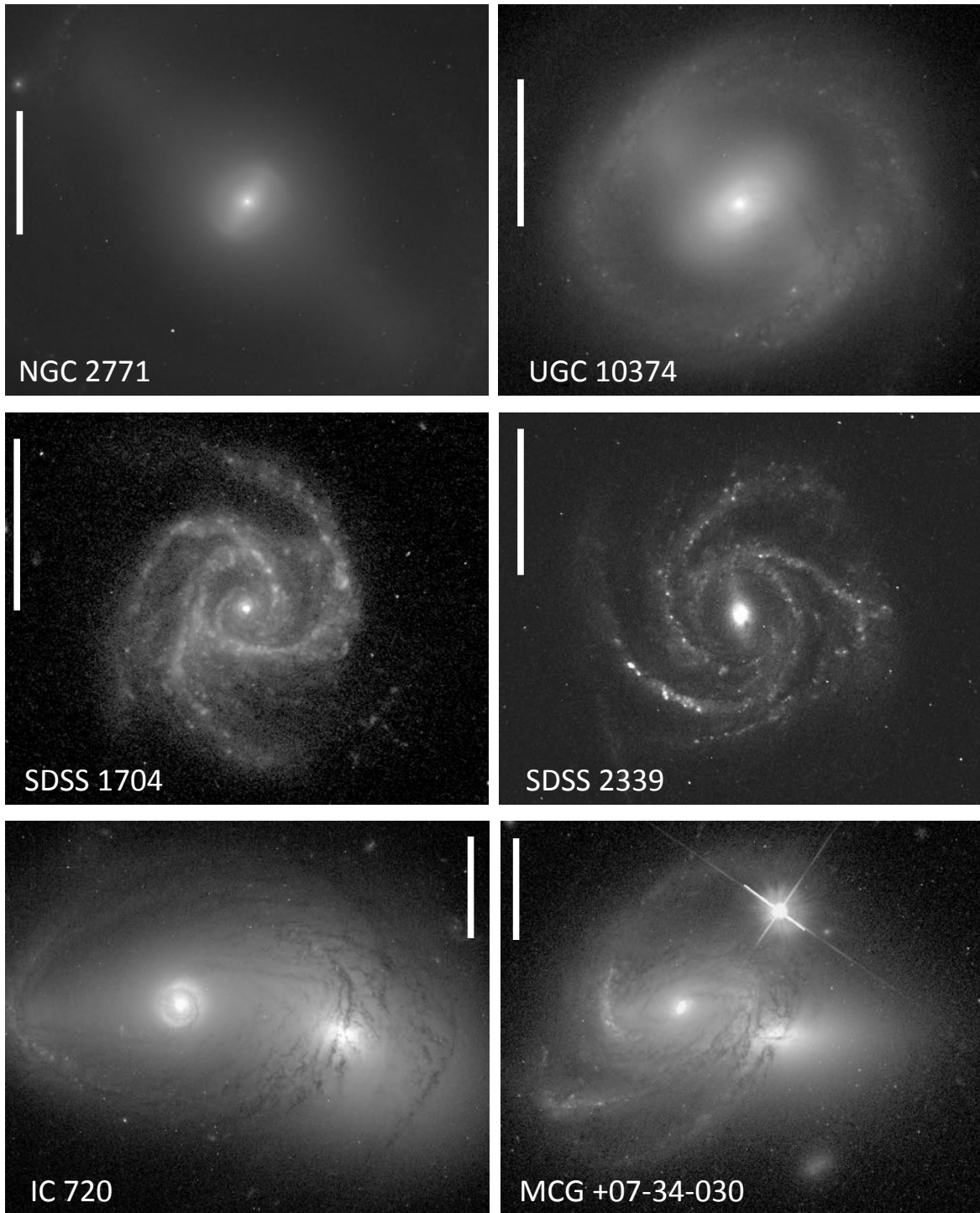
Figure 7. Some of the kinds of disk structures included in Zoo Gems data. Top row, nuclear bars and barlenses. Middle row, 3-armed spirals. Bottom row, backlit spiral arms and disk with dust attenuation. All images have north at the top and east to the left; vertical white scale bars indicate $10''$ in each case. The gray scale is logarithmic, with zero levels and contrast tailored to show the structures in each object. In the object names, SDSS destinations are truncated for legibility.

Details in the arm structures of these systems may help understand why these do not show a preference for low-density environments, as might be expected from a straightforward analysis of spiral modes after perturbation (Elmegreen et al. 1992, Hancock 2019). In SDSS J170414.33+620234.0, among the first targets observed in this program, the enhanced angular resolution of HST images reveals quite different distributions of star-forming knots along each arm, and the arms starting from an off-center ring around the core.

5.4.3. *Backlit dust*

Fig. 7 shows two of the most striking backlit-galaxy systems observed in Zoo Gems. While we will present a full modeling of these systems elsewhere, it is already noteworthy that each case shows at least thin arms of attenuation farther out than the detected starlight, and nearly transparent regions between the dust arms (and within the resonance ring in the case of IC 720). The outer dust lanes illustrate in a vivid way one advantage of dust detection with this method - arbitrarily cold dust is detectable, unlike direct far-IR measurements which rely on reradiation of absorbed starlight (Domingue et al. 1999). These images also illustrate the gain in understanding structure on going from SDSS to HST angular resolution. As has been shown with WFPC2 images of two backlit spirals (Keel & White 2001), better linear resolution reduces the confusion between unresolved dust structure and sleep of the reddening law, as there is less blending of areas with quite different attenuation. The Zoo Gems overlap systems provide a significant addition to the range of disk structures and backlit regions observed with Hubble's resolution.

5.5. *Ring features*

Among these, SDSS 133145.32+513431.2 is especially noteworthy. This object shows a subtle annular color pattern in SDSS and, more clearly, DES data (Abbott et al. 2018). The ACS image reveals a partial Einstein ring (Fig. 8), with typical radius $4.0''$, and two main segments together spanning nearly $300°$ around the brightest galaxy in a group (SDSS data give $z = 0.2894$ for this galaxy). An inflection at its northern end is associated with an individual luminous galaxy. While the source redshift remain unknown, pending further information on the lensed source and additional foreground group members, knowing the lens redshift we can bound the group mass enclosed within the Einstein ring (radius $4.0''$ or 17.5 kpc). If the source-lens distance is equal to the lens-observer distance (0.90 Gpc), the mass within 17.5 kpc would be 9×10^{12} solar masses, dropping to 3×10^{12} for the unrealistic case of arbitrarily high redshift.

5.6. *Regrowing disks*

The brightest of these are shown in Fig. 9, in comparison to two more typical advanced merging systems. The images illustrate the characteristics of two bulges, jointly surrounded by a disk with incomplete spiral patterns containing dust lanes and patchy star-forming regions.

After program submission, one of these objects (CFHTLS1220-215555) was seen to have a star superimposed on a single bulge as seen in Legacy Survey images (Dey et al. 2019), which were not clearly separated in SDSS data and appeared as a double bulge. This object does have the unusual combination of a dominant, off-center ring without a bar, and short spiral features.

The overlapping-galaxy system UGC 7064A may more exactly belong with these systems, on examination of the dust geometry. The eastern bulge component is surrounded by a ring including stars and dust, which may also encircle the inclined spiral disk to its west.

5.7. *Reassignment of galaxy categories*

Some objects turn out to be something quite different than we inferred from the SDSS or Legacy Survey images. For example, the components of the NGC 5021 system show obvious signs of tidal interaction (off-center nucleus, helical dust lanes, spokes), rather than being a superposition of relatively undisturbed galaxies. SDSS-1237668504364187727 (SDSS-J 161224.60+594610.4), observed as a potential reddened AGN with bluer outflow regions, looks like a multi-component merger; a Lick Observatory spectrum, using the Kast spectrograph at the 3m Shane telescope, shows the core to host highly reddened star formation, with relatively unreddened star formation on either side. The central region has emission-line redshift $z = 0.1019$.

6. CONCLUSIONS

We have described the diverse scientific cases addressed in the "Gems of the Galaxy Zoos" HST gap-filler program, and detailed the target selection and public input involved in its object list. The results so far illustrate the value of
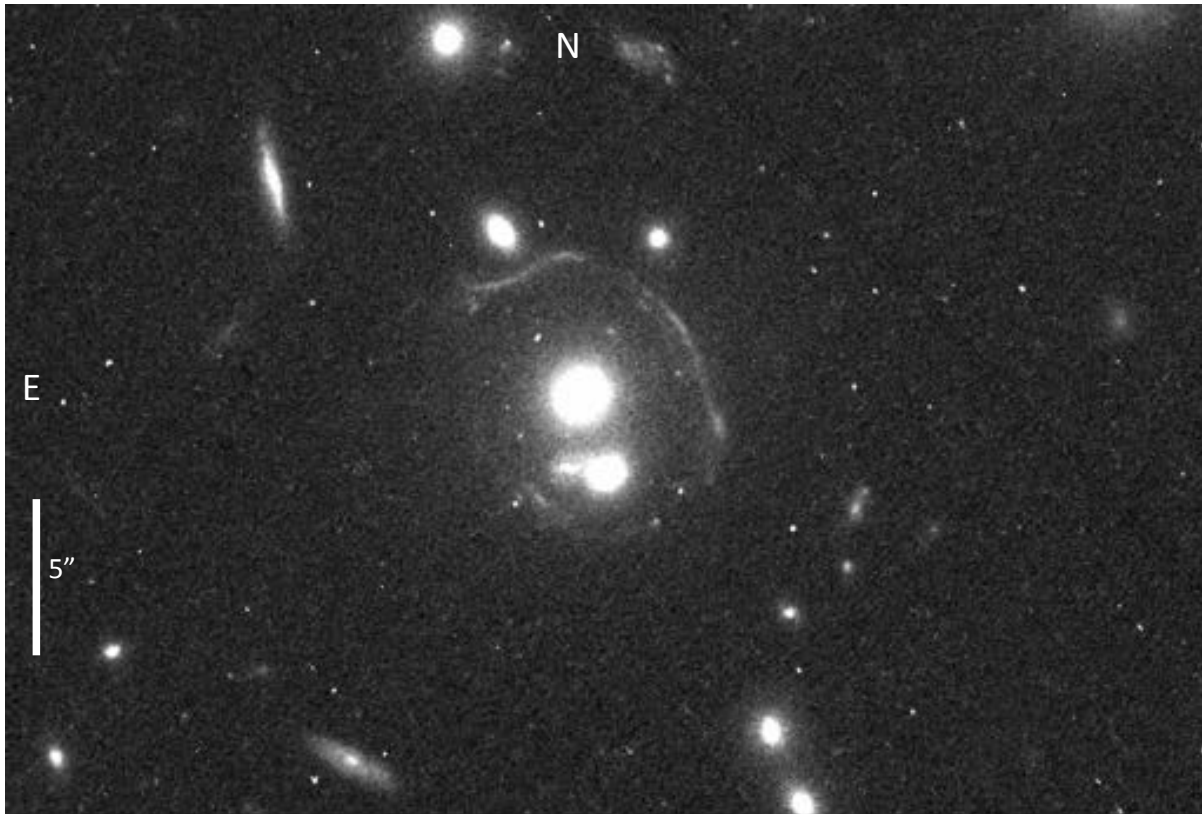
SDSS 133145.32+513431.2

Figure 8. Deep-red F814W image of the lensed arc around the central galaxy SDSS 133145.32+513431.2 ($z = 0.2894$). The upward inflection to the north may indicate perturbation by the separate potential of the bright galaxy just outside the arc. The partial ring has characteristic radius $4.0''$, projecting to 17.5 kpc at the distance of the lensing system.

even short-exposure images at Hubble's high angular resolution, deriving additional results from the effort invested by volunteers in the Galaxy Zoo and Radio Galaxy Zoo projects. These data have revealed extended redder components around Green Pea starburst systems, small-scale spiral patterns in blue early-type galaxies, and suggested that some merging galaxies quickly reform star-forming disks. Additional uses will certainly be forthcoming. The variety of results already found from this unusually wide-ranging program may encourage the community to consider ways to achieve a similar richness of use for projects on other facilities. This includes availability of high angular resolution, which has proven crucial in such applications as substructure of Green Pea starbursts, using dust attenuation to unravel the geometry of disks and merging systems, and distinguishing key morphological features such as spiral arms in radio-AGN hosts. Many of our results illustrate the complementary roles of deep survey images and even shallow high-resolution images.
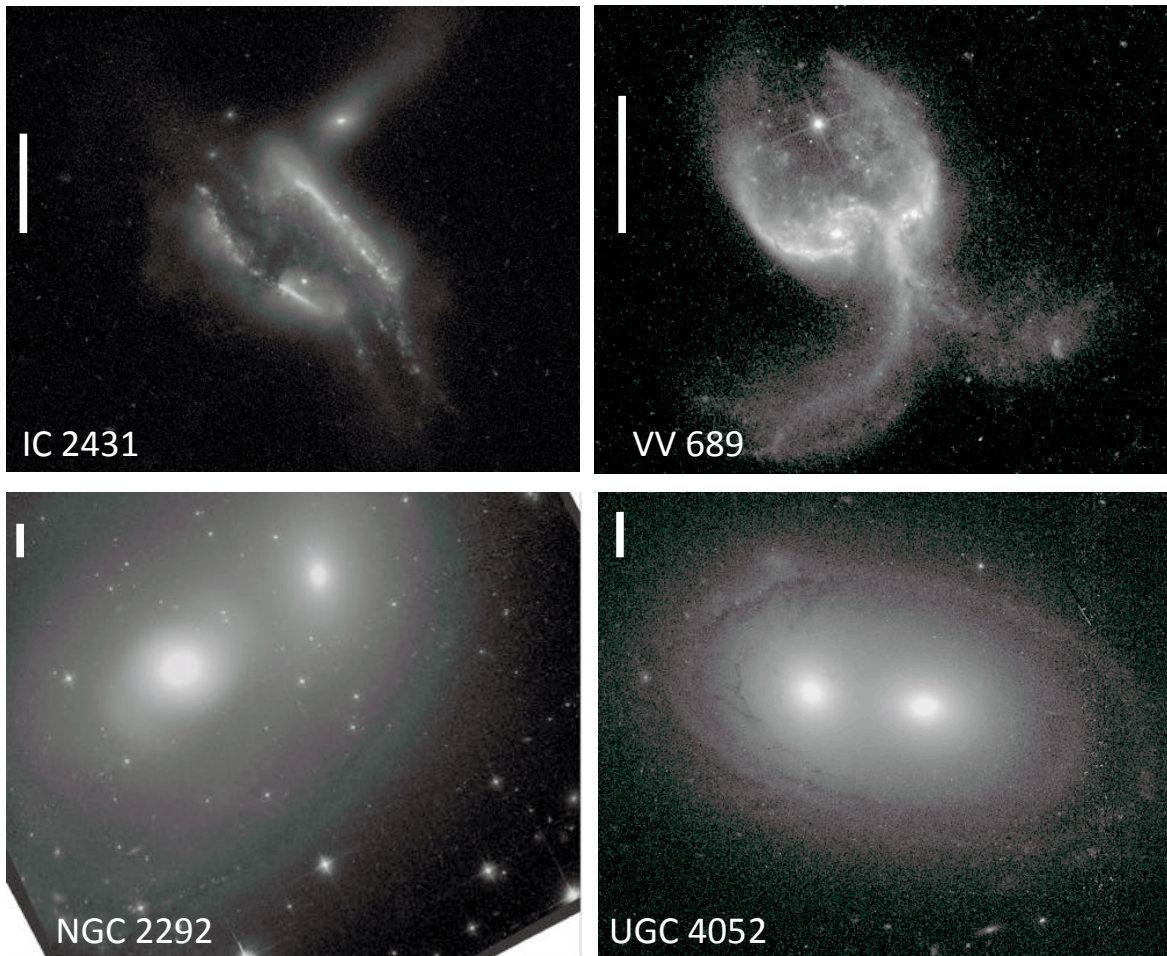
Figure 9. Montage of merging galaxies, including two typical mergers (upper row) and two potential regrowing disks (lower row). The layout is as in Fig. 7, with 10″scale bars. The regrowing disks illustrated here span large enough areas on the sky to include the stripe of cosmic-ray events across the middle, where only a single exposure was obtained as the telescope made a dither motion to give double coverage elsewhere. For NGC 2292, the edges of the ACS combined field appear in the corners.

ACKNOWLEDGMENTS

Facilities: HST(ACS), Lick(Shane)

REFERENCES

Abazajian, K. N., Adelman-McCarthy, J. K., Agüeros, M. A., et al. 2009, ApJS, 182, 543

Abbott, T. M. C., Abdalla, F. B., Allam, S., et al. 2018, ApJS, 239, 18. doi:10.3847/1538-4365/aae9f0

Amorín, R., Pérez-Montero, E., Vílchez, J. M., et al. 2012, ApJ, 749, 185

Anderson, J., & Bedin, L. R. 2010, PASP, 122, 1035

Bamford, S. P., Nichol, R. C., Baldry, I. K., et al. 2009, MNRAS, 393, 1324

Banfield, J. K., Wong, O. I., Willett, K. W., et al. 2015, MNRAS, 453, 2326

Barnes, J. E., & Hernquist, L. 1996, ApJ, 471, 115

Berlind, A. A., Quillen, A. C., Pogge, R. W., et al. 1997, AJ, 114, 107

Bizyaev, D. V., Moiseev, A. V., & Vorobyov, E. I. 2007, ApJ, 662, 304. doi:10.1086/516627

Bosch, G., Hägele, G. F., Amorín, R., et al. 2019, MNRAS, 489, 1787

Bundy, K., Bershady, M. A., Law, D. R., et al. 2015, ApJ, 798, 7. doi:10.1088/0004-637X/798/1/7

Bureau, M. & Freeman, K. C. 1999, AJ, 118, 126. doi:10.1086/300922

Cardamone, C., Schawinski, K., Sarzi, M., et al. 2009, MNRAS, 399, 1191

Clarke, L., Scarlata, C., Mehta, V., et al. 2020, arXiv:2012.07668

Cowie L. L., Hu E. M., Songaila A., 1995, AJ, 110, 1576. doi:10.1086/117631

Darg, D. W., Kaviraj, S., Lintott, C. J., et al. 2010, MNRAS, 401, 1552. doi:10.1111/j.1365-2966.2009.15786.x

Dey, A., Schlegel, D. J., Lang, D., et al. 2019, AJ, 157, 168

Domingue, D. L., Keel, W. C., Ryder, S. D., et al. 1999, AJ, 118, 1542. doi:10.1086/301062

Durbala, A., Buta, R., Sulentic, J. W., et al. 2009, MNRAS, 397, 1756

Egorov, O. V. & Moiseev, A. V. 2019, MNRAS, 486, 4186. doi:10.1093/mnras/stz1112

Elmegreen, B. G., Elmegreen, D. M., & Montenegro, L. 1992, ApJS, 79, 37

Elmegreen D. M., Elmegreen B. G., Sheets C. M., 2004, ApJ, 603, 74. doi:10.1086/381357

Elmegreen, B. G., Kaufman, M., Struck, C., et al. 2000, AJ, 120, 630

Ford, H. C., Bartko, F., Bely, P. Y., et al. 1998, Proc. SPIE, 234

Governato, F., Brook, C. B., Brooks, A. M., et al. 2009, MNRAS, 398, 312

Hancock, C. 2019, M.S. thesis, University of Alabama, https://search.proquest.com/pqdtglobal/results/6142D47E2FFC4865PQ/1?accountid=14472

Hawley, S. A. 2012, PASP, 124, 21

Hernández Toledo, H. M., Dultzin-Hacyan, D., Gonzalez, J. J., et al. 1999, AJ, 118, 108. doi:10.1086/300921

Hogarth, L., Amorín, R., Vílchez, J. M., et al. 2020, MNRAS, 494, 3541. doi:10.1093/mnras/staa851

Holwerda, B. W., Keel, W. C., Williams, B., et al. 2009, AJ, 137, 3000

Hopkins, P. F., Cox, T. J., Younger, J. D., et al. 2009, ApJ, 691, 1168

Hota, A., Sirothia, S. K., Ohyama, Y., et al. 2011, MNRAS, 417, L36

Jaskot, A. E., Oey, M. S., Scarlata, C., et al. 2017, ApJL, 851, L9

Keel, W. C., & White, R. E. 2001, AJ, 121, 1442

Keel, W. C., White, R. E., Owen, F. N., et al. 2006, AJ, 132, 2233

Keel, W. C., & White, R. E. 2001, AJ, 122, 1369

Keel, W. C., Chojnowski, S. D., Bennert, V. N., et al. 2012, MNRAS, 420, 878

Keel, W. C., Lintott, C. J., Schawinski, K., et al. 2012, AJ, 144, 66

Keel, W. C., Manning, A. M., Holwerda, B. W., et al. 2013, PASP, 125, 2

Keel, W. C., Lintott, C. J., Maksym, W. P., et al. 2017, ApJ, 835, 256

Kelvin, L. S., Bremer, M. N., Phillipps, S., et al. 2018, MNRAS, 477, 4116. doi:10.1093/mnras/sty933

Kim, K. J., Malhotra, S., Rhoads, J. E., et al. 2021, ApJ, 914, 2. doi:10.3847/1538-4357/abf833

Koss, M. J., Blecha, L., Bernhard, P., et al. 2018, Nature, 563, 214. doi:10.1038/s41586-018-0652-7

Kruk, S. J., Lintott, C. J., Bamford, S. P., et al. 2018, MNRAS, 473, 4731. doi:10.1093/mnras/stx2605

Kruk, S. J., Erwin, P., Debattista, V. P., et al. 2019, MNRAS, 490, 4721. doi:10.1093/mnras/stz2877

Laurikainen, E., Salo, H., Buta, R., et al. 2011, MNRAS, 418, 1452. doi:10.1111/j.1365-2966.2011.19283.x

Leahy, J. P. 1993, in Jets in Extragalactic Radio Sources, eds. H.-J. Röser & K. Meisenheimer (Berlin: Springer Verlag), Lect. Notes Phys. 421, 1

Ledlow, M. J., Owen, F. N., Yun, M. S., et al. 2001, ApJ, 552, 120

Lintott, C. J., Schawinski, K., Slosar, A., et al. 2008, MNRAS, 389, 1179

Lintott, C. J., Schawinski, K., Keel, W., et al. 2009, MNRAS, 399, 129

MacKenty, J.W. 2017, Space Telescope Users' Group http://www.stsci.edu/institute/stuc/fall-2017/gap.pdf

Malkan, M. A. & Malkan, B. K. 2021, ApJ, 909, 92. doi:10.3847/1538-4357/abd84e

Mao, M. Y., Owen, F., Duffin, R., et al. 2015, MNRAS, 446, 4176

Maraston, C., Strömbäck, G., Thomas, D., et al. 2009, MNRAS, 394, L107. doi:10.1111/j.1745-3933.2009.00621.x

Masters, K. L., Mosleh, M., Romer, A. K., et al. 2010, MNRAS, 405, 783

Masters K. L., Nichol R. C., Hoyle B., Lintott C., Bamford S. P., Edmondson E. M., Fortson L., et al., 2011, MNRAS, 411, 2026. doi:10.1111/j.1365-2966.2010.17834.x

Masters, K. L., Stark, D. V., Pace, Z. J., et al. 2019, MNRAS, 488, 3396. doi:10.1093/mnras/stz1889

Masters, K. L. & Galaxy Zoo Team 2020, Galactic Dynamics in the Era of Large Surveys, 353, 205. doi:10.1017/S1743921319008615

Mendez, A. J., Coil, A. L., Lotz, J., et al. 2011, ApJ, 736, 110. doi:10.1088/0004-637X/736/2/110

Moffett, A. J., Phillipps, S., Robotham, A. S. G., et al. 2019, MNRAS, 489, 2830. doi:10.1093/mnras/stz2237

Mulcahy, D. D., Mao, M. Y., Mitsuishi, I., et al. 2016, A&A, 595, L8

Mulia, A. J., Chandar, R., & Whitmore, B. C. 2016, ApJ, 826, 32. doi:10.3847/0004-637X/826/1/32

Ogle, P. M., Lanz, L., Nader, C., et al. 2016, ApJ, 817, 109. doi:10.3847/0004-637X/817/2/109

Ogle, P. M., Lanz, L., Appleton, P. N., et al. 2019, ApJS, 243, 14. doi:10.3847/1538-4365/ab21c3

Orlitová, I., Verhamme, A., Henry, A., et al. 2018, A&A, 616, A60. doi:10.1051/0004-6361/201732478

Peng, C. Y., Ho, L. C., Impey, C. D., et al. 2002, AJ, 124, 266. doi:10.1086/340952

Rampazzo, R. & Sulentic, J. W. 1992, A&A, 259, 43

Reshetnikov, V. P. & Combes, F. 1994, A&A, 291, 57

Schawinski, K., Lintott, C., Thomas, D., et al. 2009, MNRAS, 396, 818

Schawinski, K., Lintott, C. J., Thomas, D., et al. 2009, ApJ, 690, 1672

Schawinski, K., Urry, C. M., Simmons, B. D., et al. 2014, MNRAS, 440, 889. doi:10.1093/mnras/stu327

Simmons, B. D., Lintott, C., Willett, K. W., et al. 2017, MNRAS, 464, 4420. doi:10.1093/mnras/stw2587

Smethurst, R. J., Lintott, C. J., Simmons, B. D., et al. 2015, MNRAS, 450, 435. doi:10.1093/mnras/stv161

Stark, D. V., Masters, K. L., Avila-Reese, V., et al. 2021, MNRAS, 503, 1345. doi:10.1093/mnras/stab566

Thomas, D., Steele, O., Maraston, C., et al. 2013, MNRAS, 431, 1383. doi:10.1093/mnras/stt261

Toomre, A. 1977, Evolution of Galaxies and Stellar Populations, 401

Trouille, L., Lintott, C. J., & Fortson, L.F. 2019, PNAS, 116, 1902

White, R. E., Keel, W. C., & Conselice, C. J. 2000, ApJ, 542, 761

White, R. E., & Keel, W. C. 1992, Nature, 359, 129

Whitmore, B. C., Lucas, R. A., McElroy, D. B., et al. 1990, AJ, 100, 1489

Whitmore, B. C., Schweizer, F., Leitherer, C., et al. 1993, AJ, 106, 1354. doi:10.1086/116732

Willett, K. W., Lintott, C. J., Bamford, S. P., et al. 2013, MNRAS, 435, 2835

Willett, K. W., Galloway, M. A., Bamford, S. P., et al. 2017, MNRAS, 464, 4176

Wong, O. I., Schawinski, K., Kaviraj, S., et al. 2012, MNRAS, 420, 1684

Wong, O. I., Schawinski, K., Józsa, G. I. G., et al. 2015, MNRAS, 447, 3311. doi:10.1093/mnras/stu2724

Yang, H., Malhotra, S., Gronke, M., et al. 2017, ApJ, 844, 171

York, D. G., Adelman, J., Anderson, J. E., et al. 2000, AJ, 120, 1579. doi:10.1086/301513